Finite element approximation of MHD flow past a vertical plate in an embedded porous medium with a convective boundary condition and cross diffusion

Cite as: AIP Conference Proceedings **2246**, 020025 (2020); https://doi.org/10.1063/5.0015574
Published Online: 28 July 2020

Ch. Vijaya Bhaskar, Siva Reddy Sheri, and Anjan Kumar Suram

Finite Element Approximation of MHD Flow Past a Vertical Plate in an Embedded Porous Medium with a Convective Boundary Condition and Cross Diffusion

Ch. Vijaya Bhaskar [1,a)] Siva Reddy Sheri [2,b)] and Anjan Kumar Suram[3,c)]

[1]*Department of Mathematics, Vignan Institute of Technology and Science, Hyderabad, Telangana*
[2]*Department of Mathematics, GITAM University, Hyderabad Campus, Telangana, India*
[3]*Department of Mathematics, Christu Jyothi Institute of Technology and Science, Jangaon, Telangana, India*

[b)]Corresponding author: sreddy7@yahoo.co.in
[a)] vijay3284@gmail.com
[c)]anjankumar.suram@gmail.com

Abstract. Magnetohydrodynamic flow past a vertical plate in embedded porous medium with a convective boundary condition and cross diffusion through finite element approximation has been studied in the current investigation. Soret and Dufour effects are also considered. The converted dimensionless, non-linear, coupled, partial differential equations with the associated initial and boundary conditions are solved by utilizing Galerkin weighted residual method. For the recommended permeability, numerical outcomes are presented graphically against various flow pertinent parameters. Validation of finite element solutions for measure of the skin friction, heat transfer, mass transfer and surface temperature at the plate are accomplish by means of examination with the recently published work as unique instances of the present examination and extremely great relationship acquired.

Keywords: Vertical plate, Porous medium, Convective boundary condition, Cross diffusion, FEM.

INTRODUCTION

The MHD flow and heat exchange problems have received prodigious attention of the research lovers due to its abundance practical applications in rapid thermal processing, control of the fluid stream, induction heating in contactless stirring and surface modification etc. These works have explored many complex problems relevant to magnetic induction, Lorentzian body forces, magnetic levitation, AC and DC magnetic field and thermal physics. There has been an enthusiasm for analyzing MHD flow under the influence of thermal radiation because it is useful in building frameworks, ionization of fluids, numerous new designing procedures.

The corrosive and chemically-reacting nature of near-wall flows in MHD generators, also mobilizes cross-diffusion effects. These include the Soret (thermo-diffusion) effect and the Dufour (diffusion-thermo) effects. The former refers to scenarios in which lower density species and higher density species separate at the molecular level under a temperature gradient. In seeded Potassium working fluids which are popular in MHD Hall generators [1], the Soret effect is possible since generally more than one chemical species is present under a very large temperature gradient. In terms of mathematical models, this supplements the species diffusion equation (concentration boundary

International Conference on Mathematical Sciences and Applications (ICMSA-2019)
AIP Conf. Proc. 2246, 020025-1–020025-14; https://doi.org/10.1063/5.0015574
Published by AIP Publishing. 978-0-7354-2005-2/$30.00

layer equation) with extra thermal diffusion terms. The Dufour effect describes the energy (heat) flux created when a chemical system is subjected to a significant concentration gradient and may also arise in corrosive boundary layer zones of MHD generators. To simulate this phenomenon, the energy conservation equation has to be augmented with supplementary species diffusion terms.

Numerous researchers have investigated Soret and Dufour phenomena in both viscous hydrodynamics and magnetohydrodynamics (although generally in the absence of Hall currents in MHD). Representative studies in this regard include Li et al. [2] (who also considered endothermic reactions), Siva Reddy Sheri et al. [3] (transient hydromagnetic dissipative flow), Pandya and Shukla [4] (high temperature Hall magneto-gas dynamics), Siva Reddy Sheri and Prasanthi [5] (double-diffusive reactive time-dependent MHD) and Majeed et al. [6] (viscoelastic ferromagnetic boundary layers).

Heat and mass transfer by laminar free convection through a vertical plate was explored by so many investigators due to its applications. Several computational studies of reactive MHD boundary layer flows with heat and mass transfer have presented by various authors such as Makinde [7], Makinde and Sibanda [8], Makinde and Ogulu [9], Beg et al. [10], Ahmad et al. [11], Merkin and Chaudhary [12], Makinde [13], Bataller [15] , Sadeq and Sayyed [16] , Siva Reddy and Anjan Kumar [17] , Siva Reddy et al. [18], Siva Reddy and Prasanthi [19] , Siva Reddy et al. [20], Siva Reddy et al. [21] and Vijaya Bhaskar et al [22].

In light of the above works, it is evident that no investigation took place to find thermal radiation, heat source, Soret and the Dufour effects. In this investigation Magnetohydrodynamic flow past a vertical plate in embedded porous medium with a convective boundary condition and cross diffusion is studied. Solutions of the current considered problem are presented graphically. Local skin friction, the plate surface temperature and the local heat and mass transfer rates are displayed with the aid of tables. The results are believed to be applicable to realistic engineering situations cited earlier.

MATHEMATICAL FORMULATION

A steady, laminar, hydromagnetic coupled heat and mass transfer by mixed convection flow of a cold fluid at temperature T_∞ over an infinite vertical plate embedded in a porous medium is considered. The left surface of the plate heated by convection from a hot fluid with temperature T_f which provides a heat transfer coefficient h_f . The other opposite surface of the fluid is assumed to be cold, Newtonian and electrically conducting. All other fluid properties except density are assumed to be independent of temperature and chemical species concentration. A uniform magnetic field of strength B_0 is imposed normal to the plate(along the $y-$ axis) as shown in Fig.1.Since the magnetic Reynolds number is very small for most fluid used in industrial applications, we assume that the induced magnetic field is negligible.

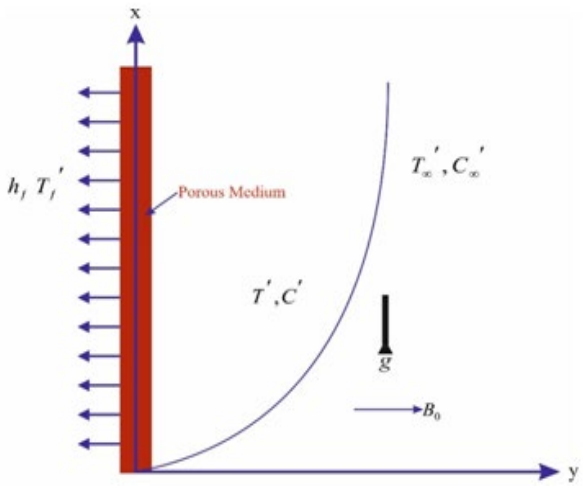

FIGURE 1. Flow Configuration and coordinate system of the Problem

$$-v_w \frac{\partial u'}{\partial y'} = v\frac{\partial^2 u'}{\partial y'^2} + g\beta_t (T' - T'_\infty) + g\beta_m (C' - C'_\infty) + \frac{\sigma B_0^{\,2}}{\rho}(U' - u') + \frac{v}{k}(U' - u') \tag{1}$$

$$-v_w \frac{\partial T'}{\partial y'} = \frac{k}{\rho C_p}\frac{\partial^2 T'}{\partial y'^2} + \frac{v}{C_p}\left(\frac{\partial u'}{\partial y'}\right)^2 + \frac{\sigma B_0^{\,2}}{\rho C_p}\left(U' - u'\right)^2 - \frac{1}{\rho C_P}\frac{\partial q_r}{\partial y} - \frac{Q_0}{\rho C_P}\left(T' - T'_\infty\right) + \frac{\rho D_m K_T}{c_s}\frac{\partial^2 C'}{\partial y'^2} \tag{2}$$

$$-v_w \frac{\partial C'}{\partial y'} = D\frac{\partial^2 C'}{\partial y'^2} - \gamma\left(C' - C'_\infty\right) + \frac{D_m K_T}{T_m}\frac{\partial^2 T'}{\partial y'^2} \tag{3}$$

The associated boundary conditions are given by:

$$y = 0 : u = 0; \quad -k\frac{\partial T'}{\partial y} = h_f\left(T_f - T\right); \quad C = C_\infty \tag{4}$$

$$y \to \infty : u \to U; \quad T \to T_\infty; \quad C \to C_\infty \tag{5}$$

where u is the velocity, v, C_P and k are kinematic viscosity, specific heat at constant pressure and thermal conductivity of the fluid, respectively. β_t and β_m are thermal and concentration expansion coefficients. g, q_r, v_m, C_w and U are the gravitational acceleration, radiation heat flux, wall suction velocity, local concentration at plate surface and free stream velocity, respectively. σ is the electrical conductivity and k is the permeability parameter. Subscript ∞ the free stream conditions of temperature and concentration. Furthermore, D is the mass diffusivity, T_m is the mean fluid temperature, K_p is the thermal diffusion ratio, C_s is the concentration susceptibility and γ is the reaction rate coefficient.

By taking into account the Rosseland approximation for the radiation term in the equation (2), the convective heat flux q_r, can be modeled as:

$$q_r = -\frac{4\sigma^*}{3k^*}\frac{dT^4}{dy} \tag{6}$$

where k^* is the Rosseland mean absorption coefficient and σ^* is the Stefan-Boltzmann constant. The Rosseland approximation is used for an optically thick medium, so the fluid is assumed to be optically thick medium. It seems reasonable to assume that the temperature differences within the flow are sufficiently small so that, T^4 can be stated in a simpler way by using a Taylor series about T_∞ and neglecting higher order terms, therefore:

$$T^4 \cong 4T_\infty{}^3 T - 3T_\infty^4 \tag{7}$$

By replacing the above expression into equations (6) and (7), the energy equation (2) reduces to

$$-v_w\frac{dT}{dy} = \frac{k}{\rho C_p}\frac{d^2T}{dy^2} + \frac{\nu}{C_p}\left(\frac{du}{dy}\right)^2 + \frac{\sigma B_0{}^2}{\rho C_p}(U-u)^2 + \frac{16\sigma^* T_\infty^3}{3\rho C_P k^*}\frac{d^2T}{dy^2} + \frac{\rho D_m K_T}{c_s}\frac{\partial^2 C'}{\partial y'^2} \tag{8}$$

To normalize the equations (1), (3), to (5) and (8), the following normalized quantities are introduced:

$$\left\{\begin{array}{l} \eta = \dfrac{v_w y}{\nu},\ \ \mathrm{Pr} = \dfrac{\rho\eta C_P}{k}\ ,\ E_C = \dfrac{v_w^2}{C_P\left(T_f - T_\infty\right)},\ f = \dfrac{u}{v_w}\ ,\ S_c = \dfrac{\nu}{D}\ ,\ \lambda = \dfrac{\gamma\nu^2}{Dv_w^2},\ \ \theta = \dfrac{T-T_\infty}{T_f - T_\infty}, \\ R = \dfrac{4\sigma^* T_\infty^3}{kk^*},\ Gr = \dfrac{g\beta_t\left(T_f - T_\infty\right)\nu}{v_w^3},\ \varphi = \dfrac{C - C_\infty}{C_w - C_\infty},\ \ G_c = \dfrac{g\beta_m\left(C_w - C_\infty\right)\nu}{v_w^3},\ \ F = \dfrac{U}{v_m}, \\ K = \dfrac{v_w{}^2 k}{\nu^2},\ \ M = \dfrac{\sigma B_0^2\nu}{\rho c},\ Bi = \dfrac{h_f\nu}{kv_m},\ Q = \dfrac{\nu Q_0}{\rho C_P U_0{}^2}\ Sr = \dfrac{D_m K_T\left(T'_w - T'_\infty\right)}{T_m\nu\left(C'_w - C'_\infty\right)},\ Du = \dfrac{D_m K_T\left(C'_w - C'_\infty\right)}{c_s c_p\nu\left(T'_w - T'_\infty\right)} \end{array}\right\} \tag{9}$$

The calculations of *y* direction are considered while the variations are neglected in the *x* direction. Therefore, with help of normalized parameters the ordinary differential equations (1), (3) to (5) and (8) are converted to simplified ordinary differential equations as follows:

$$-\frac{df}{d\eta} = \frac{d^2 f}{d\eta^2} + Gr\theta + Gc\phi + M(F-f) + \frac{F-f}{k} \tag{10}$$

$$-\frac{d\theta}{d\eta} = \frac{1}{\mathrm{Pr}}\left(1 + \frac{4R}{3}\right)\frac{d^2\theta}{d\eta^2} + Ec\left(\frac{df}{d\eta}\right)^2 + MEc(F-f)^2 - Q\theta + Du\frac{\partial^2 C}{\partial y^2} \tag{11}$$

$$-\frac{d\phi}{d\eta} = \frac{1}{Sc}\frac{d^2\phi}{d\eta^2} - \frac{\lambda}{Sc}\phi + Sr\frac{\partial^2\theta}{\partial y^2} \tag{12}$$

$$\eta = 0 : f = 0;\ \frac{d\theta}{d\eta} = Bi[\theta - 1];\ \phi = 1$$
$$\eta \to \infty :\ f = F;\ \theta = \phi = 0 \tag{13}$$

From the engineering point of view, the skin-friction coefficient and also the Nusselt number is given by:

$$C_f = \frac{2}{F^2} f'(0) \tag{14}$$

$$Nu = \frac{hv}{kv_w} = \frac{T_f - T_\infty}{T_w - T_\infty} \theta'(0) = -\frac{\theta'(0)}{\theta(0)} \tag{15}$$

Where T_w is the plate surface temperature and the Sherwood number is given by:

$$Sh = \frac{h_m v}{Dv_w} = -\phi'(0) \tag{16}$$

Where h_m is the convection mass transfer coefficient.

METHOD OF SOLUTION

Transformed non-dimensional flow governing partial differential equations (10)–(12) along with boundary conditions (13) are solved numerically by adopting FEM with Galerkin weighted residual scheme. This method comprises five fundamental steps, namely discretization of the domain, derivation of the element equations, assembly of element equations, imposition of boundary conditions and finally iterative scheme is employed to solve the matrix system, which is solved using Gauss elimination method, maintaining an accuracy of 10^{-7}. The detailed description of this method is explained by Bathe[23] and Reddy[24].

VALIDATION OF NUMERICAL SOLUTION

In order to authenticate and check the present numerical method and results we made a comparison with available results of Makinde and Aziz [14] and Sadeq and Sayyed [16] exhibited in Tables 1. This table exhibits the comparison of skin-friction $f'(0)$, Nusselt number $-\theta'(0)$ and Sherwood number $-\phi'(0)$ for Biot number (Bi) and it is recognized that there is good agreement between the results exist.

TABLE 1. Comparison of values of $f'(0), -\theta'(0), -\phi'(0)$ when $(R = 0,\ Q = 0,\ Sr = 0\ and\ Du = 0)$

Bi	Makinde and Aziz [14]			Sadeq and Sayyed [16]			Present results		
	$f'(0)$	$-\theta'(0)$	$-\phi'(0)$	$f'(0)$	$-\theta'(0)$	$-\phi'(0)$	$f'(0)$	$-\theta'(0)$	$-\phi'(0)$
0	1.892	0.000	0.459	1.888	0.000	0.459	1.891	0.000	0.459
1	1.908	0.398	0.459	1.904	0.398	0.459	1.902	0.398	0.459
10	1.917	0.639	0.459	1.914	0.639	0.459	1.913	0.639	0.459

TABLE 2. Values of $\phi'(0), u'(0), \theta'(0)$ and $\theta(0)$

Bi	M	K	Ec	R	Q	Sc	Kr	Du	Sr	$-\phi'(0)$	$u'(0)$	$-\theta'(0)$	$\theta(0)$
0	0.1	0.1	0.1	1.0	1.0	0.24	0.1	1.0	1.0	0.46153	1.79145	0.00000	0.05371
0.1	0.1	0.1	0.1	1.0	1.0	0.24	0.1	1.0	1.0	0.46153	1.79571	0.09135	0.17398
1.0	0.1	0.1	0.1	1.0	1.0	0.24	0.1	1.0	1.0	0.46153	1.81362	0.42764	0.61524
10	0.1	0.1	0.1	1.0	1.0	0.24	0.1	1.0	1.0	0.46153	1.83742	0.67143	0.95041
0.1	1.0	0.1	0.1	1.0	1.0	0.24	0.1	1.0	1.0	0.46153	1.86435	0.09352	0.17802
0.1	10	0.1	0.1	1.0	1.0	0.24	0.1	1.0	1.0	0.46153	2.41938	0.09039	0.21057
0.1	0.1	1.0	0.1	1.0	1.0	0.24	0.1	1.0	1.0	0.46153	0.78132	0.09469	0.15683
0.1	0.1	10	0.1	1.0	1.0	0.24	0.1	1.0	1.0	0.46153	0.76254	0.09473	0.14965
0.1	0.1	0.1	1.0	1.0	1.0	0.24	0.1	1.0	1.0	0.46153	1.82753	0.05841	0.60235
0.1	0.1	0.1	2.0	1.0	1.0	0.24	0.1	1.0	1.0	0.46153	1.84621	0.00093	1.27431
0.1	0.1	0.1	0.1	2.0	1.0	0.24	0.1	2.0	2.0	0.46153	1.88232	0.26583	0.163589
0.1	0.1	0.1	0.1	3.0	1.0	0.24	0.1	3.0	3.0	0.46153	1.91091	0.44871	0.551288
0.1	0.1	0.1	0.1	1.0	2.0	0.24	0.1	1.0	1.0	0.46153	0.92015	0.08625	0.991347
0.1	0.1	0.1	0.1	1.0	3.0	0.24	0.1	1.0	1.0	0.46153	0.23012	0.08174	0.144253
0.1	0.1	0.1	0.1	1.0	1.0	0.62	0.1	1.0	1.0	0.82781	1.78965	0.09137	0.17031
0.1	0.1	0.1	0.1	1.0	1.0	0.78	0.1	1.0	1.0	0.98423	1.78674	0.09139	0.16978
0.1	0.1	0.1	0.1	1.0	1.0	0.24	1.0	1.0	1.0	0.92678	1.78201	0.091347	0.17261
0.1	0.1	0.1	0.1	1.0	1.0	0.24	2.0	1.0	1.0	1.35741	1.78013	0.091351	0.17256
0.1	0.1	0.1	0.1	1.0	1.0	0.24	0.1	2.0	1.0	0.62341	1.81965	0.091324	0.17034
0.1	0.1	0.1	0.1	1.0	1.0	0.24	0.1	3.0	1.0	0.81412	1.38613	0.091342	0.16878
0.1	0.1	0.1	0.1	1.0	1.0	0.24	0.1	1.0	2.0	0.62678	1.85201	0.091315	0.17231
0.1	0.1	0.1	0.1	1.0	1.0	0.24	0.1	1.0	3.0	0.90021	1.92013	0.091332	0.17211

RESULTS AND DISCUSSION

A comprehensive parametric investigation has been accomplished to know the variations in the profiles of velocity, temperature and concentration. Effects of dissimilar parameters on Skin friction, Nusselt number and Sherwood number are also investigated. In current investigation the following values have adopted for numerical calculations.

$$Gr = Gc = 1.0, M = 0.1, K = 1.0, \Pr = 0.72, Ec = 0.1, Bi = 0.1, R = 1.0, Q = 1.0, Du = 1.0,$$
$$Sr = 1.0, Sc = 0.62, Kr = 0.1, F = 0.5$$

The Biot number (Bi) is a ratio of internal conduction resistance within solid to external convection resistance at body surface.

Figs 2 and 3 explains the influence of Biot number on velocity and temperature. Fig 2 clarifies that without Bi the peak velocity is low. This is because of the reason that as the convection Biot number increases, the plate thermal resistance reduces. Fig. 3 excesses that temperature on the right side of the plate increases with an increase in the Biot number, since as Bi increases, the thermal resistance of the plate decreases and convective heat transfer to the fluid on the right side of the plate increase.

Thermal Grashof number is the ratio of buoyancy to viscous forces in the boundary layer, fig 4 reveals that velocity get accelerated on rising Gr due to buoyancy force. The same result is identified with mass transfer Grashof number shown in fig.5. It is interesting to note that for Gc=3 that is, for high concentration between the wall and the free stream, the vertical component of the velocity in a portion of the boundary layer is large than unity which implies that the vertical velocity exceeds the wall suction velocity.

Fig. 6. Shows the impact of M on velocity. It is determined that, the velocity decreases with the rise of the M, as a results of the essence of a magnetic field in associate with electrically conducting fluid introduces a force referred to as the Lorentz force, that acts against the flow if the magnetic field is applied within the normal direction. This resistive force reduced the fluid velocity. Influence of porosity parameter K on velocity is demonstrated in fig.7. It explains that the K enhances the upward flow profoundly and shifts the location of the peak velocity further away from the plate.

The Prandtl number is the ratio of momentum diffusivity to thermal diffusivity. From the Fig. 8 it is clear that a rise in $\Pr$ from 0.025 to1.38 causes a decrease in velocity. The result of $\Pr$ on temperature is shown in Fig.9. Rising of $\Pr$ reduces the thermal boundary layer thickness. In heat transfer issues, the $\Pr$ controls the relative momentum and thermal boundary layer thickness. Fluids with lower $\Pr$ have higher thermal conductivity, so heat will diffuse from the sheet quicker than for higher $\Pr$. Hence, Prandtl number can be used to increase the speed of cooling in conducting flows.

Effect of viscous dissipation (Eckert number) on velocity and temperature profiles are shown in Figs. 10. and 11 respectively. The relationship between the kinetic energy in the flow and the enthalpy is given by Eckert number. It represents the exchange of kinetic energy into internal energy by work done against the viscous fluid stresses. Larger viscous dissipative heat causes a growth in the temperature as well as the velocity.

Figs. 12. and 13. illustrate the influence of the heat absorption coefficient Q on the velocity and temperature profiles. It is identified that both the profiles get decelerated on increasing Q. It conveys that absorption (thermal sink) has the tendency to reduce the fluid temperature and velocity.Figures 14 and 15 illustrate the progress in velocity and temperature with the radiation- parameter (R), respectively. Significant enhancement in velocity and

temperature is identified with induced values of R. Momentum boundary layer thicknesses are therefore reduced whereas thermal boundary layer thickness is elevated with increasing radiation parameter.

The velocity profiles $f(\eta)$ against dissimilar values of Schmidt numbers, namely, hydrogen ($Sc = 0.24$), water vapor ammonia ($Sc = 0.78$) and propyl benzene ($Sc = 2.62$), are shown in Fig. 16. It indicates that velocity get decelerated on increasing Sc. Similarly the influence of Sc on concentration profile is explained in Fig. 17. For every value of Sc, the dimensionless concentration declines from a value of one at the plate to a value of zero at the edge of the concentration boundary layer. As Sc increases, the species concentration drops more rapidly as the thickness of the concentration boundary layer decreases. Since the increase in Sc implies a decrease in the molecular diffusion D the concentration decay over a shorter distance is understandable. Similarly, one would anticipate that the heavier species (higher Sc) would have a shorter penetration depth (thinner boundary layer).

Figs 18. and 19. present the effects of chemical reaction rate parameter Kr on velocity profiles $f(\eta)$ and concentration distributions $\varphi(\eta)$. An increase in the values of Kr, decreases the velocity profiles as seen in Fig 18. From Fig19, it is very clear that the reactive solutal ofile decrease with a rise in the values of Kr . That is, the reaction rate parameter is a decreasing agent and as a result, the solute boundary layer close to the wall becomes thinner. This is as a result of the change of species which is experienced near the wall due to the presence of chemical reaction and then decreases the concentration in the boundary layer.

Figs 20 and 21 exhibit the velocity and temperature profiles for different values of Dufour number Du. The Dufour number Du denotes the contribution of the concentration gradient, $\partial^2 C / \partial y^2$ to the thermal energy flux in the flow. It can be seen that an increase in the Dufour number causes a rise in velocity (fig. 20) and temperature (fig. 21) throughout the boundary layer. Concentration gradients, via coupling between the energy eqn. (11) and species eqn. (12) clearly reduce hydrodynamic boundary layer thicknesses whereas they elevate thermal boundary layer thickness.

Figs 22 and 23 visualize the impact of the Soret (thermo-diffusion) number (Sr) on the velocity and concentration profiles are plotted in respectively. The Soret number Sr defines the effect of the temperature gradients inducing significant mass diffusion effects and is featured in the second order linear derivative term in eqn. (15), viz $\mathrm{Sr}(\partial^2 \theta / \partial y^2)$. Increasing Soret number Sr clearly elevates both the primary and secondary velocity magnitudes and furthermore also boosts the species concentration magnitudes. Both momentum boundary layer thicknesses are decreased whereas the species boundary layer thickness is enhanced. Inclusion of both Dufour and Soret cross-diffusion effects therefore exert a non-trivial influence on transport characteristics along the duct wall (plate). Absence of these effects results in a substantial under-prediction in primary and secondary velocity (without Dufour effect), under-prediction in species concentration (without Soret effect) and over-prediction in velocity magnitude (without Soret effect).

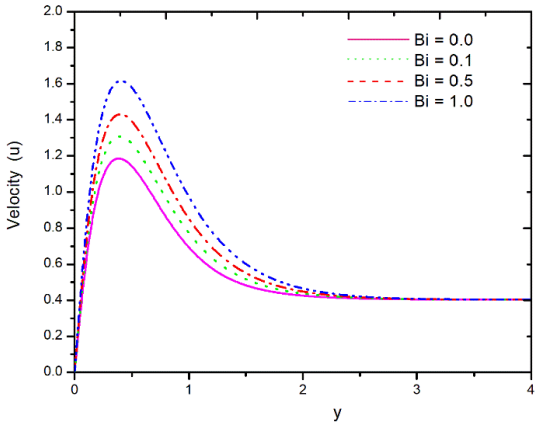

Fig 2. Effect of Bi on velocity profile

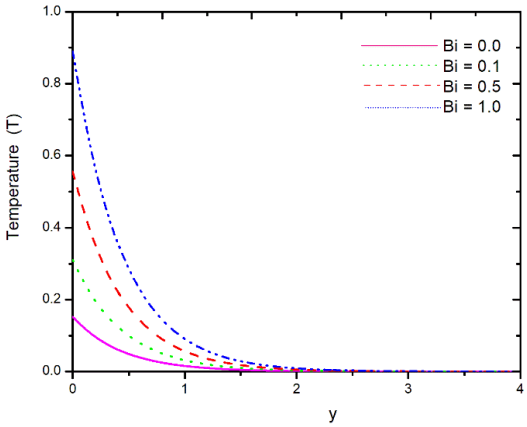

Fig 3. Effect of Bi on temperature profile

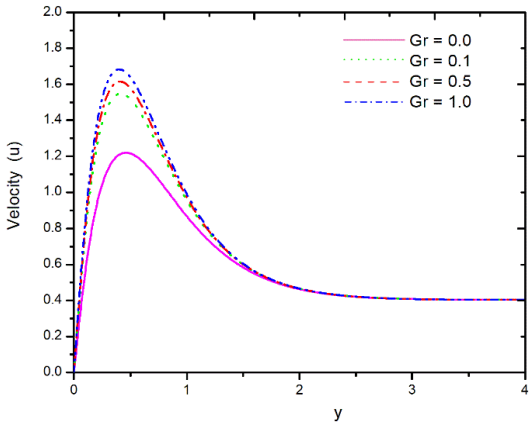

Fig 4. Effect of Gr on velocity profile

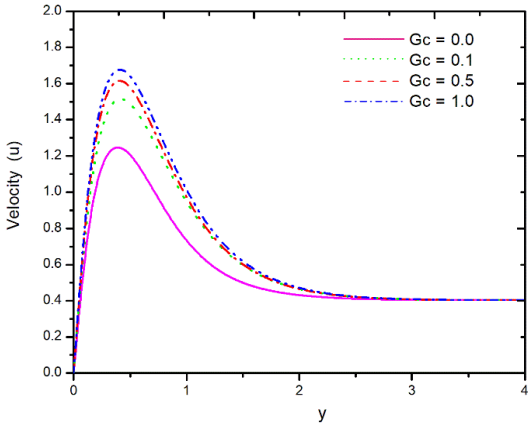

Fig 5. Effect of Gc on velocity profile

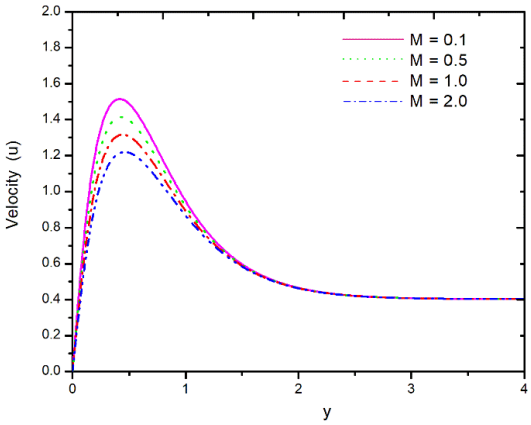

Fig 6. Effect of M on velocity profile

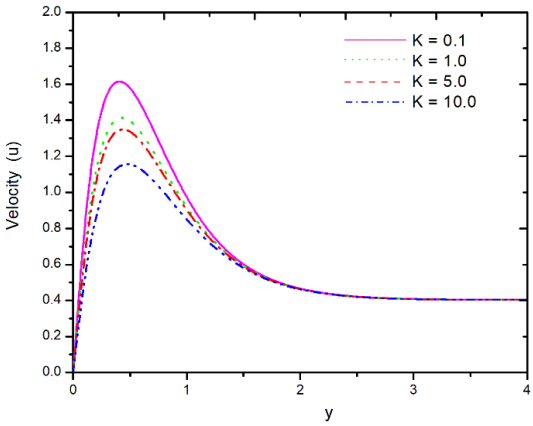

Fig 7. Effect of K on velocity profile

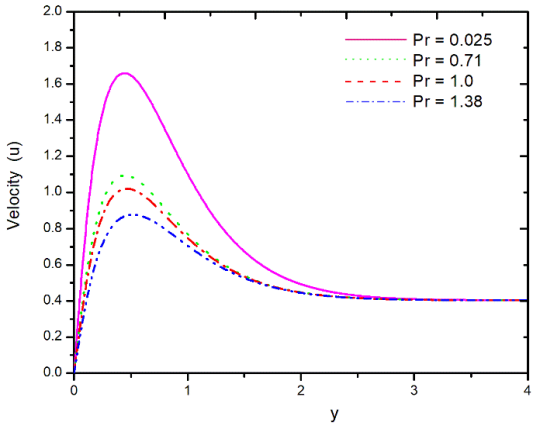

Fig 8. Effect of Pr on velocity profile

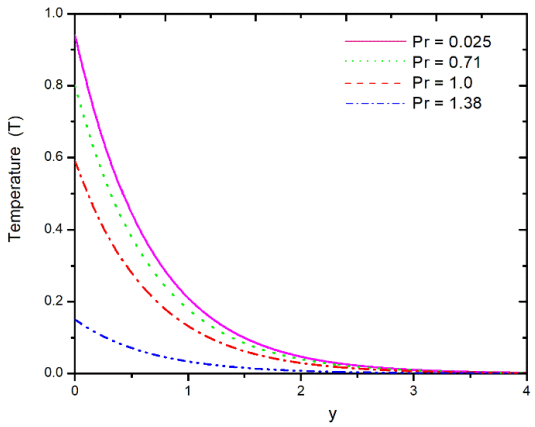

Fig 9. Effect of Pr on temperature profile

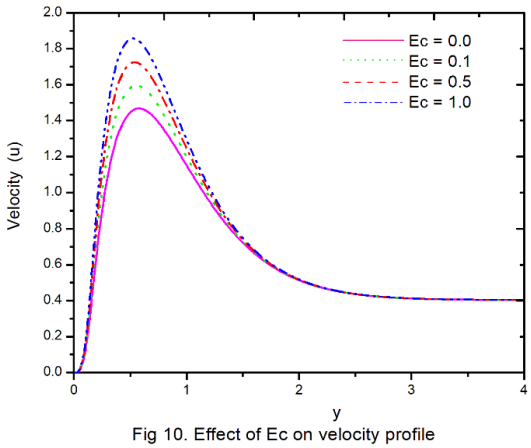

Fig 10. Effect of Ec on velocity profile

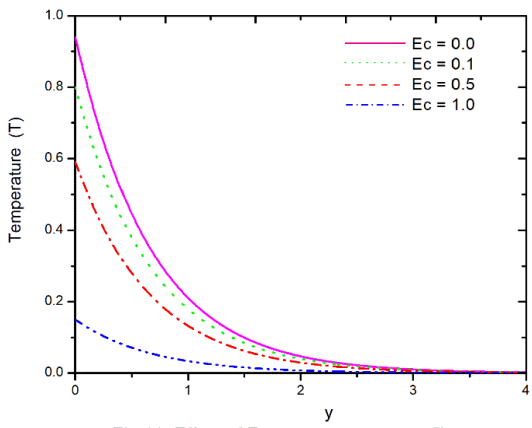

Fig 11. Effect of Ec on temperature profile

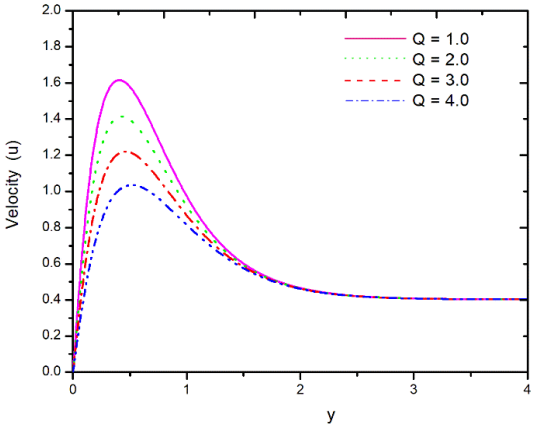

Fig 12. Effect of Q on velocity profile

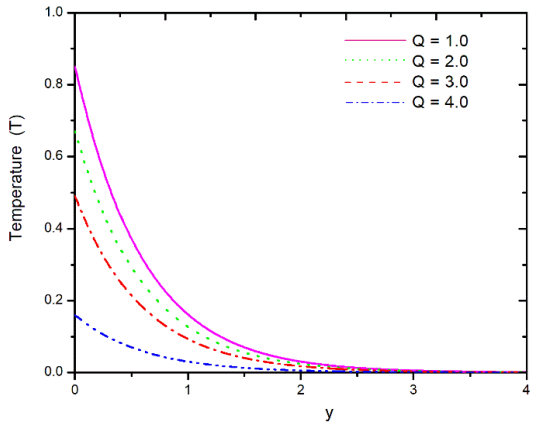

Fig 13. Effect of Q on temperature profile

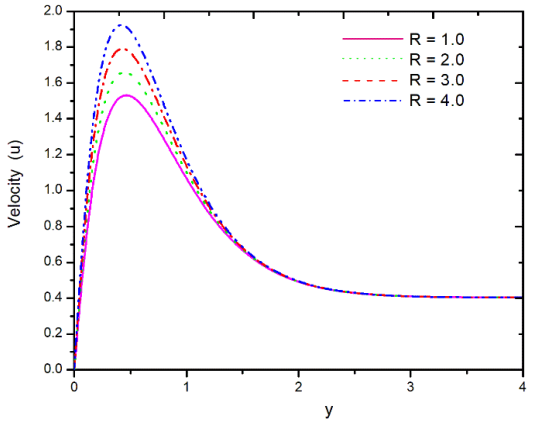

Fig 14. Effect of R on velocity profile

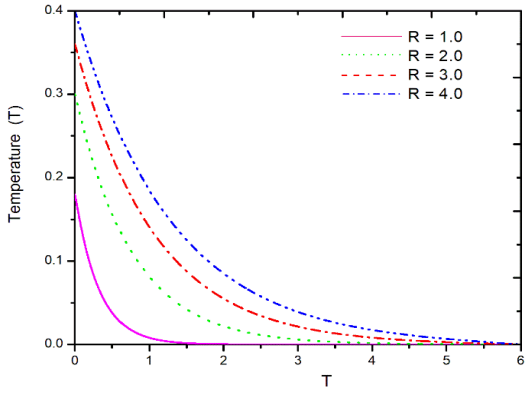

Fig 15. Effect of R on temperature profile

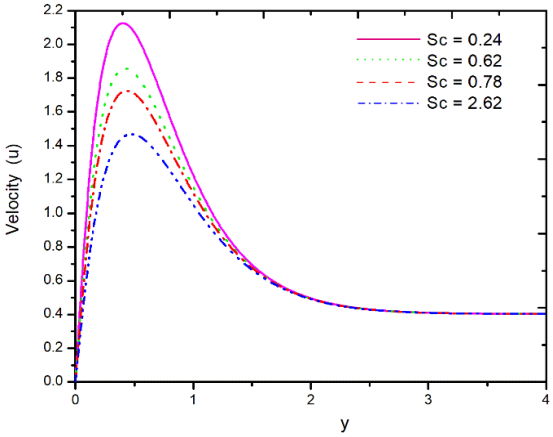

Fig 16. Effect of Sc on velocity profile

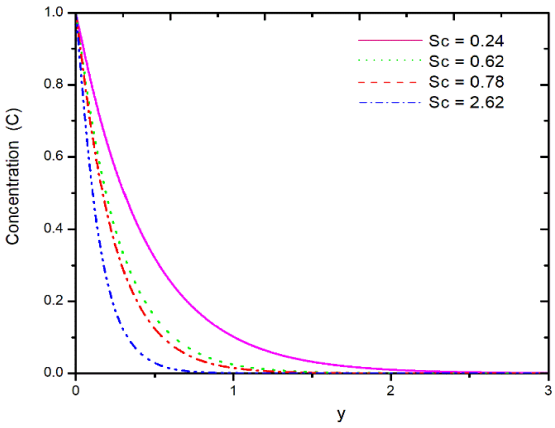

Fig 17. Effect of Sc on concentration profile

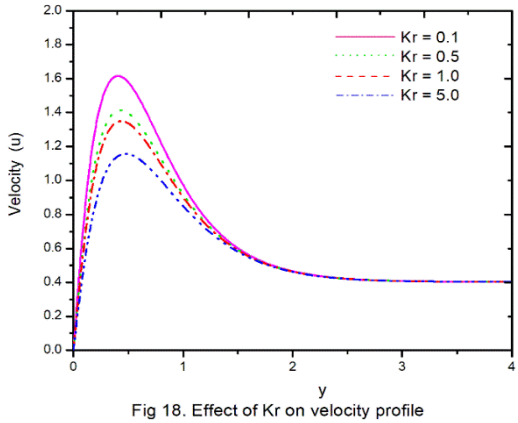

Fig 18. Effect of Kr on velocity profile

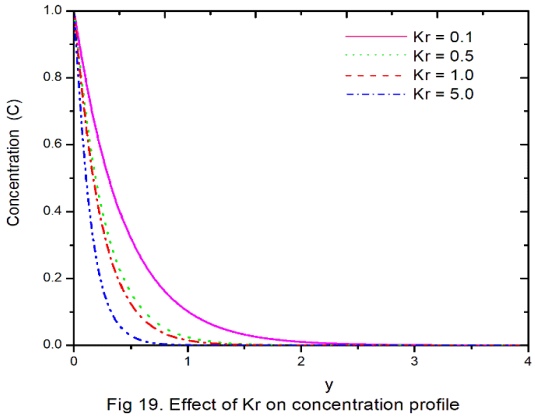

Fig 19. Effect of Kr on concentration profile

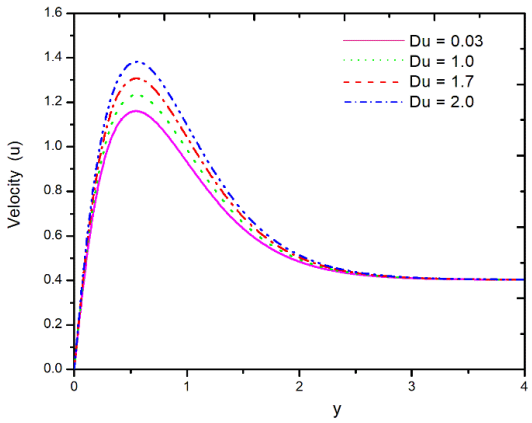

Fig 20. Effect of Du on velocity profile

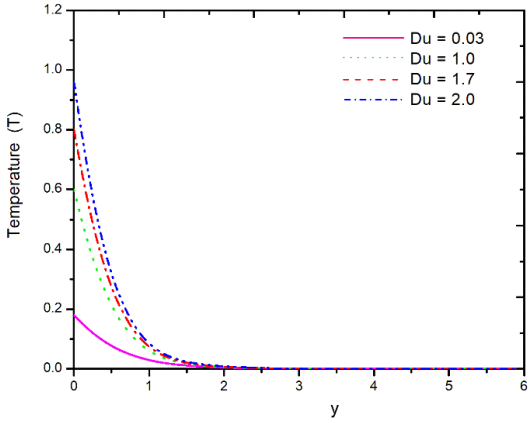

Fig 21. Effect of Du on temperature profile

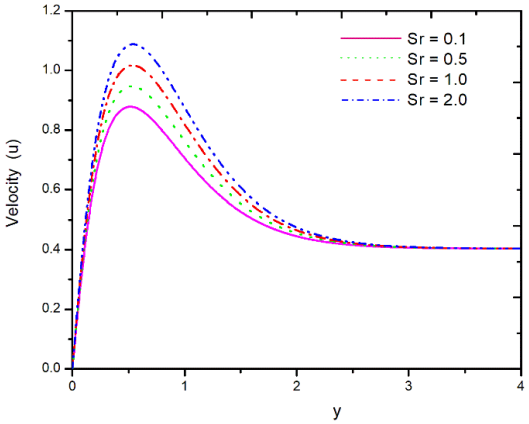

Fig 22. Effect of Sr on velocity profile

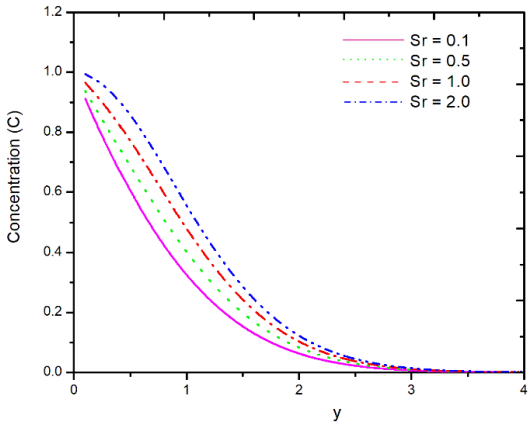

Fig 23. Effect of Sr on concentration profile

Skin Friction, Heat Transfer (Nusselt Number), Mass Transfer (Sherwood Number) Parameters and Surface Temperature:

The quantities $u'(0), \theta'(0), \phi'(0)$ are measure of the skin friction, heat transfer, and mass transfer at the plate, respectively, while the quantity $\theta(0)$ gives the plate surface temperature. Table-2 records the values of these quantities for a range of values of the parameters $Bi, M, K, Ec, R, Q, Sc, Kr, Du \text{ and } Sr$. The skin friction $u'(0)$ increases as the Biot number Bi, the Eckert number Ec, Magnetic parameter M, Thermal radiation R, increase but decreases when Permeability parameter K, Heat absorption Q, Schmidt number Sc, Chemical reaction Kr and Soret (thermo-diffusion) number (Sr) increase. The heat transfer rate $-\theta'(0)$ from the plate increases with the increase in values of Bi, K, R, Sc, Du and Kr but decreases with the increase in M, Ec, Q and Sr. The mass transfer is seen to increase with the increase in Sc, Kr and Sr and mass transfer parameters $-\phi'(0)$ are not affected with increase in the Bi, M, K, Ec, R, Q and Du. Surface temperature $\theta(0)$ increases with the increase in values of Bi, M, Ec, R, Du, Sr but decreases with the increase in K, Q, Sc and Kr. For $Bi = 0$, no convective heat transfer takes place and the rate of heat transfer at the plate surface is zero as expected.

CONCLUSIONS

In this paper, we studied the MHD mixed convective flow past vertical plate in embedded porous medium with a convective boundary condition. The dimensionless equations are solved numerically by using finite element method. The most significant findings of the present study are as follows.

The results demonstrated that, the values of velocity and temperature are enhanced with increasing the Biot number.

We found that the velocity is enhanced with an increase in thermal Grashof number, mass Grashof number, permeability parameter, viscous dissipation (Eckert number), thermal radiation Dufour and Soret number. The reverse trend is observed with increasing Magnetic parameter, Prandtl number, heat absorption, Schmidt number and chemical reaction rate parameter.

It is conclude that an increase in the thermal radiation,Viscous dissipation and Dufour number leads to an enhancement in temperature and thermal boundary layer thickness. The opposite behavior is identified with increasing Heat absorption parameter.

We fascinated that, Schmidt number, chemical reaction rate parameter and Soret number tend to decelerate species concentration .

The obtained numerical solutions are compared with previously published results and are found to be in excellent agreement.

REFERENCES

1. N.J.S. Maken, and B.Gupta, Energy Conversion and Management,21,115-120(1981).
2. M.C Li.,Y.W.Tian, and Y.C. Zhai, Transactions of Nonferrous Metals Society of China,16,1200–1204(2006).
3. Siva Reddy Sheri and R.Srinivasa Raju, International Journal Computational Methods in Engineering Science and Mechanics,16,132-141(2015).
4. N. Pandya, and A.K. Shukla, TWMS J. App. Eng. Math, 6,163-174(2016).
5. Siva Reddy Sheri, and Prasanthi Modugula, International Journal of Applied and Computational Mathematics, 3,1289-1306(2017).
6. A. Majeed, A.Zeeshan, R.Ellahi, Engineering Science and Technology- International Journal,20,1122-1128(2017). http://dx.doi.org/10.1016/j.jestch.2016.11.007 .
7. O.D.Makinde, Applied Thermal Engineering,29, 1773-1777(2009).
8. O.D.Makinde, and P.Sibanda, ASME e Journal of Heat Transfer,130, 11260 (1-8) (2008).
9. O.D.Makinde, and A. Ogulu, Chemical Engineering Communications,195 (12), 1575-1584(2008).
10. O.A. Beg, J. Zueco, R.Bhargava, and H.S.Takhar, International Journal of Thermal Sciences,48, 913-921(2009).
11. S. Ahmad, N.M. Arifin, R.Nazar, and I.Pop, International Journal of Thermal Sciences,48, 1943-1948(2009).
12. J.H. Merkin, and M.A.Chaudhary, Quarterly Journal of Mechanics and Applied Mathematics,47, 405-428(1994).
13. O.D.Makinde, International Journal of Numerical Methods for Heat & Fluid Flow, 19 (3,4), 546-554(2009).
14. O.D.Makinde, and A. Aziz, International Journal of Thermal Sciences,49, 1813–1820(2010).
15. R.C.Bataller, Applied Mathematics and Computation, 206, 832-840(2008).
16. Sadeq Zafariyan, and Sayyed Aboozar Fanaee, Journal of Science and Engineering(Cankaya University), 10(1), 123–136(2013).
17. Siva Reddy Sheri and S.Anjan Kumar, Procedia Engineering (Elsevier, Scopus),127,893-900(2015).

18. Siva Reddy Sheri, and S.Anjan Kumar, Journal of Applied Science and Engineering,19,385-392(2016).
19. Siva Reddy Sheri, S.Anjan Kumar, and Prasanthi Modugula, Journal of the Korean Society for Industrial and Applied Mathematics, 20, 355–374(2016).
20. Siva Reddy Sheri, and Prasanthi Modugula, International Journal of Applied and Computational Mathematics, 3, 1289-1306(2017).
21. Siva Reddy Sheri, Ali J.Chamkha, and S.Anjan Kumar, International Journal of Numerical Methods for Heat & Fluid Flow, 27(11), 2541-2480(2017).
22. Ch.Vijaya Bhaskar, Siva Reddy Sheri, and S.Anjan Kumar, ARPN Journal of Engineering and Applied Sciences,13(22),8846–8853(2018).
23. K.J. Bathe, Finite Element Procedures, (New Jersey:.Prentice-Hall, 1996).
24. J.N. Reddy, An Introduction to the Finite Element Method, (3rd Edition, New York: McGraw-Hill Book Company, 2006).